COBEM 2023 27TH INTERNATIONAL CONGRESS OF MECHANICAL ENGENEERING

ABCM Brazilian Society of Mechanical Sciences and Engineering
27th ABCM International Congress of Mechanical Engineering
December 04-08, 2023, Florianópolis-SC, Brazil

COB-2023-1953
EXPERIMENTS OF FLOW-INDUCED VIBRATION ON MODELS IN REGIMES OF LOW REYNOLDS NUMBERS: PART 2 – SQUARE-COLUMNS ARRANGEMENTS

Adriana Porto Wallbach
Karen Gomes Soares
Gabriel de Paula Dittrich
André Luís Condino Fujarra
Laboratório de Interação Fluido-Estrutura – LIFE
Federal University of Santa Catarina – UFSC, Joinville / SC, Brazil
adriana.wallbach@posgrad.ufsc.br
karen.soares@grad.ufsc.br
gabriel.dittrich@grad.ufsc.br
andre.fujarra@ufsc.br

Abstract. *In addition to circular columns, Semi-Submersible Platforms (SSP) or Floating Offshore Wind Turbines (FOWT) also feature columns with square sections. This geometry is easily modularized during construction, making it an attractive choice from a constructive point of view. Regarding the phenomenon of FIV, square-section columns exhibit different behaviors at different angles of flow incidence, some of them eventually with lower amplitudes of vibration. Therefore, to seek a better solution for column arrangements, square-section geometries should also be considered, not just circular ones. Due to the large number of conditions to be considered, Part 2 of this work was conducted to provide a more complete analysis comprising the arrangements of columns with square sections. Once again, experiments were carried out in the Circulating Water Channel (CWC) at LIFE-UFSC-Joinville to analyze the FIV phenomenon on ultrareduced models of arrangements composed of three or four square columns. For comparison purposes, the distances S between the cylinders were determined by the width D of their square cross section, also with ratios of $S/D = 2$, 3 and 4. Also, to maintain the investigative approach, the same aspect ratio $T/D = 2$ (where T is the column draft) and the same reduced mass $m^* \approx 1.83$ were considered in this second part. In terms of incident flow directions, angles of attack of 0, 90 and 180 degrees were tested for three-column arrangements and 0 and 45 degrees for the four-column arrangements. The experiments were carried out at the same seven different reduced velocities, ranging from 4.69 to 11.87. In-line and cross-flow displacements were captured through the Motion Capture System (MCS), to determine dimensionless amplitudes and frequencies. Data were processed and analyzed through computational routines in Octave, using techniques of statistics and uncertainty, as well as Fourier analysis. Comparative analyzes with equivalent results found in experimental studies with higher Reynolds numbers and numerical studies validate this work, and therefore it was concluded that CWC experiments with low Reynolds numbers are an effective, economical, and faster approach to evaluate floater arrangements of SSP and FOWT, reconfirming the original contribution stated in Part 1 of this work.*

Keywords: *Flow-Induced Vibration (FIV), Low Reynolds Numbers, Square-Columns Arrangements, Circulating Water Channel (CWC), Ultra-Reduced Models, Two Degrees of Freedom*

1. INTRODUCTION

Considering the complexity of the variables to be carefully analyzed in relation to each column arrangement and the different geometries involved, as well as the considerable number of experiments to be performed, a second part of this study was carried out to provide a comprehensive analysis. This additional approach is essential to understand in detail the numerous conditions, also taking into account arrangements of square columns, which allows a complete and refined evaluation of the study in question.

The square-section geometry offers remarkable flexibility during the construction of real floaters, making it a highly attractive option in terms of costs and therefore a highly attractive option in the field of engineering. In fact, its adaptability during construction stages confers numerous advantages, making it a prominent choice in terms of efficiency and constructive practicality.

In the case of short cylinders (columns) with a square section, among the FIV phenomena, Vortex-Induced Vibration (VIV) and Galloping stand out. According to Fujarra *et al.* (2012), the VIV of such structures is a particular case that may deserve the alternative designation of Vortex-Induced Motion (VIM), widely found in the literature. In fact, although

VIM presents similarities in the FSI mechanism, namely in terms of its self-excited and self-controlled behavior, it can differ substantially with regard to low mass and aspect ratios, m^* and AR, at very high Reynolds numbers Re, making the different designation more appropriate for this type of FIV on large offshore floating structures.

The galloping of long towers, bridges, and cables, on the other hand, has been a well-known phenomenon for years, fairly well described in Blevins (2001) and Paidoussis *et al.* (2013), to name a few. According to these references, this is a form of aeroelastic or hydroelastic instability identified by the presence of large oscillation amplitudes perpendicular to the flow direction in structures with asymmetric cross sections. This phenomenon tends to occur in structures that have relatively low structural stiffness and damping, subjected to sufficiently high-velocity flows.

Although VIM and galloping relevance have increased in recent years, mainly due to SSP and FOWT, experimental investigations on the flow around short (low aspect ratio) free-to-oscillate square-section cylinders are still scarce in the literature. For example, in Nemes *et al.* (2012) the influence of the square section cylinder attack angle on the cross-flow vibration is investigated. According to the authors, at incidence angles where the cylinder of a square section and low mass ratio aligns symmetrically with the flow, two independent vibratory mechanisms act, VIV and gallop. Alternatively, when this symmetry is broken, a combined response appears with amplitudes greater than those of each phenomenon acting separately at the same velocity. Furthermore, as the velocity increases, the response frequency splits into two different branches until, for even higher velocities, desynchronized oscillations come into existence. The transition between VIV and galloping occurs over a narrow range of angles.

To the best of the authors' knowledge, no work was found experimentally investigating FIV phenomena of square-section columns with two degrees of freedom (2dof), nor arrangements of them, in low Reynolds number regimes.

Despite this, it is known that the use of arrangements with 2dof composed of three or four columns of a square section must also imply possible combinations of VIV and galloping, even more complex than those identified for a single cylinder. In the arrangements, vortex shedding occurs around each column, with possible interference between wakes, highly affected by the angle of incidence, which should make the identification of FIV phenomena extremely difficult.

To understand this problem and complement the investigations presented in Part 1, FIV tests were now carried out with ultra-reduced models of arrangements of square section columns with 2dof in CWC in low Reynolds number regimes. By opting for an eminently experimental methodology, we again seek to obtain results to directly investigate the problem in question, as well as to promote the selection of the best cases for further investigations via CFD in full-scale Reynolds numbers, also considering that the same experimental results they can also serve to validate numerical simulation models at low Reynolds numbers, with the advantage of clarifying the flow models responsible for the dynamics.

2. METHODOLOGY

In this Part 2, the FIV tests were carried out with the same experimental setup described in Bruner *et al.* (2023). Therefore, the information that follows only describes specific aspects of square section column arrangements.

Again, to allow a direct comparative analysis of the results, all arrangements composed of three or four square section columns were kept with the aspect ratio $AR = 2$ and mass ratio $m^* = 1.83$. The distances between the centers of the columns are determined by the characteristic dimension of the cross section, in integer multiples of this measure, $S/D = 2$, 3 and 4. The models for each arrangement considered can be seen in Figure 1.

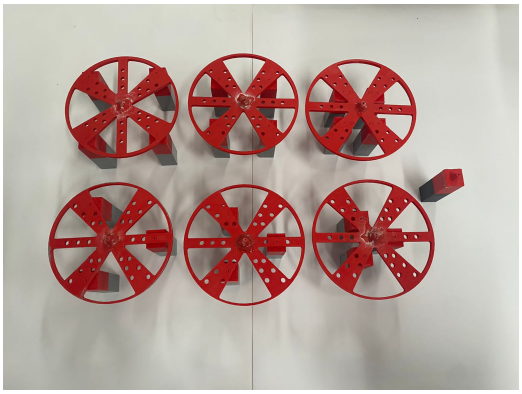

Figure 1. Small-scale models of the circular cylinder arrangements.

The experiments were carried out with the same two degrees of freedom (2dof): X direction (inline) and Y direction (cross-flow). Furthermore, for each relative distance between columns, different angles of attack were considered, namely 0° 90° and 180° for the three-column arrangements, and 0° and 45° for the four-column arrangements.

The models were tested at the same seven different uniform flow velocities U, depending on the depth of water in the CWC, now resulting in Reynolds numbers ranging from 597.5 to 1317.5, as described in Table 1.

Table 1. List of drafts, flow velocities, and tested Reynolds numbers of the Square Cylinder.

Water depth (mm)	Velocity, U (m/s)	Reynolds number
150	0.0527	1317.5
175	0.0445	1112.5
200	0.0374	935.0
225	0.0329	822.5
250	0.0302	755.0
275	0.0260	650.0
300	0.0239	597.5

Table 2 contains the series of 315 tests comprising combinations of arrangements, the relative angle to the flow, the distances between columns, and the respective reduced velocities. Once again, each condition was repeated three times, with at least 5 minutes per acquisition, which is enough to register more than 60 cycles of the FIV. As for Part 1, note again that each arrangement has its natural frequency f_n, which implies slightly different ranges of reduced velocity, where $Vr = U/(f_n \cdot D)$.

Table 2. Matrix of 105 tests repeated three times each.

Number of columns	Angle of attack	S/D	Reduced velocity, Vr	$f_n(Hz)$
3	0°	2	5.24 ; 5.70 ; 6.32 ; 7.21 ; 8.20 ; 9.76 ; 11.56	0.22
3	90°	2	5.24 ; 5.70 ; 6.32 ; 7.21 ; 8.20 ; 9.76 ; 11.56	0.22
3	180°	2	5.24 ; 5.70 ; 6.32 ; 7.21 ; 8.20 ; 9.76 ; 11.56	0.22
4	0°	2	5.19 ; 5.64 ; 6.25 ; 7.14 ; 8.12 ; 9.66 ; 11.44	0.24
4	45°	2	4.82 ; 5.24 ; 5.81 ; 6.63 ; 7.54 ; 8.97 ; 10.63	0.25
3	0°	3	5.38 ; 5.86 ; 6.49 ; 7.41 ; 8.42 ; 10.02 ; 11.87	0.23
3	90°	3	5.38 ; 5.86 ; 6.49 ; 7.41 ; 8.42 ; 10.02 ; 11.87	0.23
3	180°	3	5.38 ; 5.86 ; 6.49 ; 7.41 ; 8.42 ; 10.02 ; 11.87	0.23
4	0°	3	5.15 ; 5.60 ; 6.21 ; 7.09 ; 8.06 ; 9.59 ; 11.36	0.23
4	45°	3	4.96 ; 5.40 ; 5.98 ; 6.83 ; 7.77 ; 9.24 ; 10.94	0.24
3	0°	4	5.33 ; 5.80 ; 6.43 ; 7.34 ; 8.35 ; 9.93 ; 11.76	0.22
3	90°	4	5.33 ; 5.80 ; 6.43 ; 7.34 ; 8.35 ; 9.93 ; 11.76	0.22
3	180°	4	5.33 ; 5.80 ; 6.43 ; 7.34 ; 8.35 ; 9.93 ; 11.76	0.22
4	0°	4	5.29 ; 5.75 ; 6.37 ; 7.28 ; 8.27 ; 9.85 ; 11.66	0.23
4	45°	4	5.02 ; 5.46 ; 6.05 ; 6.91 ; 7.86 ; 9.35 ; 11.07	0.24

Information was collected using Optitrack MCS, as described in Bruner *et al.* (2023). The data obtained undergo a process of analysis and processing using computational algorithms, employing statistical analysis techniques and the Fast Fourier Transform (FFT). Through these algorithms, the absolute values of the maximum and minimum displacements were determined, as well as the mean of the 10-percent-largest values. The results are presented in a dimensionless way, related to the characteristic dimension of the cross section: $A_x^{10\%}/D$ for the X direction (inline) and $A_y^{10\%}/D$ for the Y direction (cross-flow).

The frequency analyzes were performed using FFT. As in Part 1, the dominant frequencies were determined by the value of the highest spectral density in the PSD graph. The results are shown in the same dimensionless way, $f_x^* = f_x/f_n$ and $f_y^* = f_y/f_n$, where f_x is the frequency in the X direction (inline), f_y is the frequency in the Y direction (cross flow), and f_n is the natural frequency of the arrangement, as in Table 2.

3. RESULTS AND DISCUSSIONS

As in Bruner *et al.* (2023), graphs for comparisons between dimensionless amplitudes and frequencies of the FIV were also constructed for arrangements with three or four columns of square section, simultaneously presented as a function of the relative distance S/D and reduced velocities Vr.

In a slightly different approach, in this Part 2 the analyzes were conducted in a slightly different way where the results are grouped and discussed according to amplitudes and frequencies (inline and cross-flow) for each number of columns and flow incidence.

Figure 2 shows the dimensionless amplitudes $A_y^{10\%}/D$ and $A_x^{10\%}/D$ in (a) and (c), and dimensionless frequencies $f_y^* = f_y/f_n$ and $f_x^* = f_x/f_n$ in (b) and (d), all results for an arrangement composed of three columns of square section, considering an angle of 0°. According to these results, the largest amplitudes of FIV occur in the cross-flow direction.

The $A_y^{10\%}/D$ values ranged from 0.40 and 0.85, for $5 < Vr < 12$.

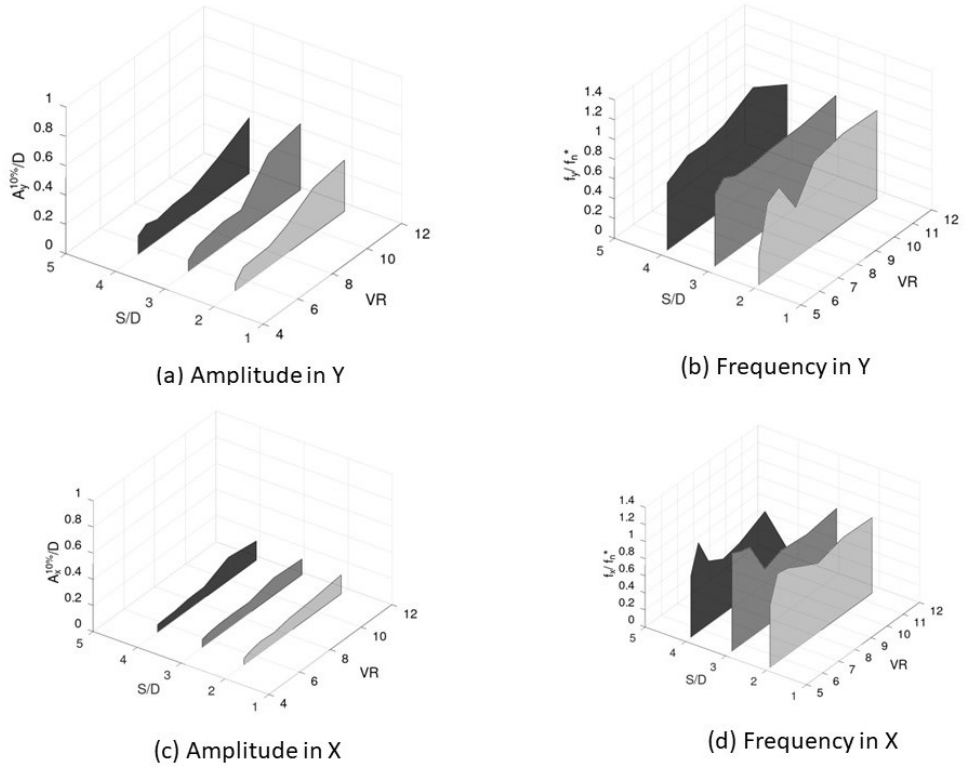

Figure 2. Results of 3-column arrays with $\theta = 0°$: (a) $A_y^{10\%}/D$, (b) $f_y^* = f_y/f_n$, (c) $A_x^{10\%}/D$ in, and (d) $f_x^* = f_x/f_n$.

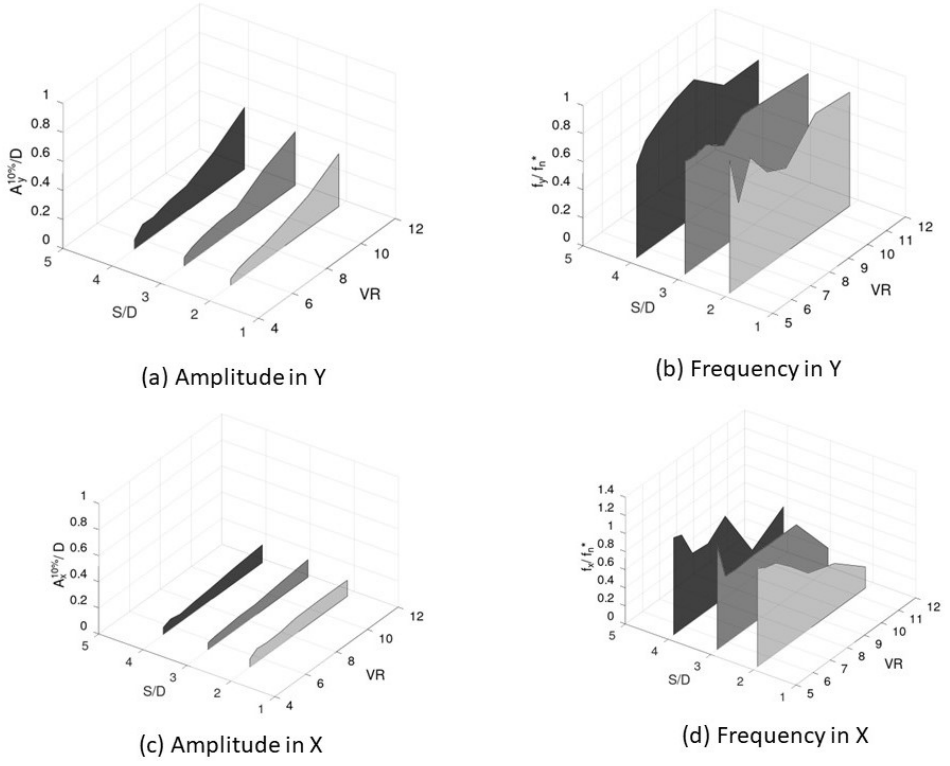

Figure 3. Results of 3-column arrays with $\theta = 180°$: (a) $A_y^{10\%}/D$, (b) $f_y^* = f_y/f_n$, (c) $A_x^{10\%}/D$ in, and (d) $f_x^* = f_x/f_n$.

It is noteworthy that the highest amplitude values are concentrated in the range of $10 < Vr < 12$. The results of amplitudes in the cross-flow direction corroborate the existence of a resonant behavior in the VIV/VIM of SSP and FOWT. The occurrence of the same behavior is observed in arrangements composed of three columns with an angle of 180°, as illustrated in Figure 3 (a). Regardless of the incidence angle, the dimensionless amplitudes in the inline direction $A_x^{10\%}/D$ show similar behavior for all relative distances between columns S/D, see Figs. 2 (c) and 3 (c).

In terms of dimensionless frequencies, Figs. 2 (b) and 3 (b) for $S/D = 2$ seem to indicate some loss of synchronization at $7 < Vr < 8$, which needs to be further investigated by means of Particle Image Velocimetry (PIV) experiments and/or CFD simulations.

Also for the arrangements with three columns of square cross section, Figure 4 shows the dimensionless amplitudes $A_y^{10\%}/D$ and $A_x^{10\%}/D$ in (a) and (c), and dimensionless frequencies $f_y^* = f_y/f_n$ and $f_x^* = f_x/f_n$ in (b) and (d), but now considering an angle of 90°of flow incidence.

According to Figs. 4 (b) and (d) for $S/D = 3$ and 4, it seems to exist two resonant mechanisms of excitation: one involving the two columns in tandem, and another related to the adjacent isolated column. In the ratio $S/D = 2$, due to the proximity between the columns, it can be considered that the three columns form a single body, with the occurrence of FIV as that on a single column.

In terms of dimensionless amplitudes $A_y^{10\%}/D$, Figure 4 (a), for the case where $S/D = 3$ and 4, small amplitudes are observed for reduced velocities lower than 8, and moderate amplitudes above this value, with a smooth transition between tandem array mechanisms and a single column. In the case of $S/D = 2$, small amplitudes are observed throughout the range of Vr.

In terms of dimensionless amplitudes $A_y^{10\%}/D$, Figure 4 (a), for the case where $S/D = 4$, moderate amplitudes are observed throughout the range of Vr, with a smooth transition between tandem array mechanisms and a single column. For $S/D = 3$, the tandem mechanism is more intense, with greater amplitudes in the range of lower V_R. In the case of $S/D = 2$, the mechanisms decrease and increase as the cylinders are approached or removed, with a single column mechanism being predominant, but maintaining the presence of the tandem arrangement.

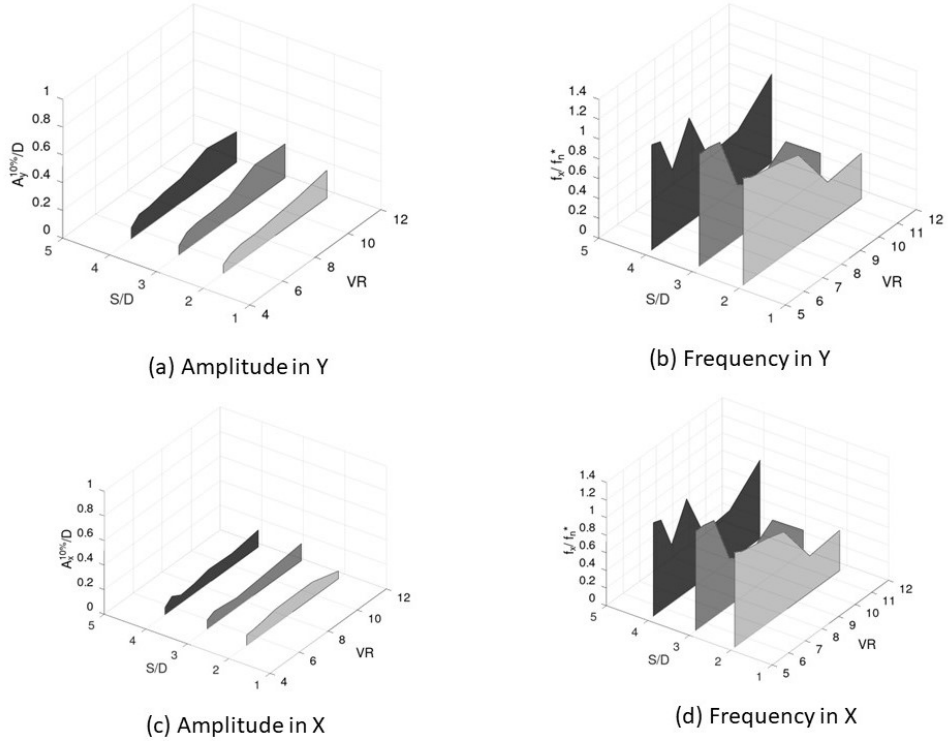

Figure 4. Results of 3-column arrays with $\theta = 90°$: (a) $A_y^{10\%}/D$, (b) $f_y^* = f_y/f_n$, (c) $A_x^{10\%}/D$ in, and (d) $f_x^* = f_x/f_n$.

Figure 5 illustrates the results of the dimensionless amplitudes (a) and (c) and dimensionless frequencies (b) and (d) for inline and cross-flow directions of arrangements with four columns of square section, considering an angle of 0°of flow incidence. According to Figs. 5 (b) and (d), it seems that again there are two synchronization mechanisms, one at higher reduced velocities (Vr from 7 to 10), and another at lower values (Vr from 4 to 7). In terms of dimensionless amplitudes $A_y^{10\%}/D$, the values are lower than those for three-column arrangements in the same angle of incidence.

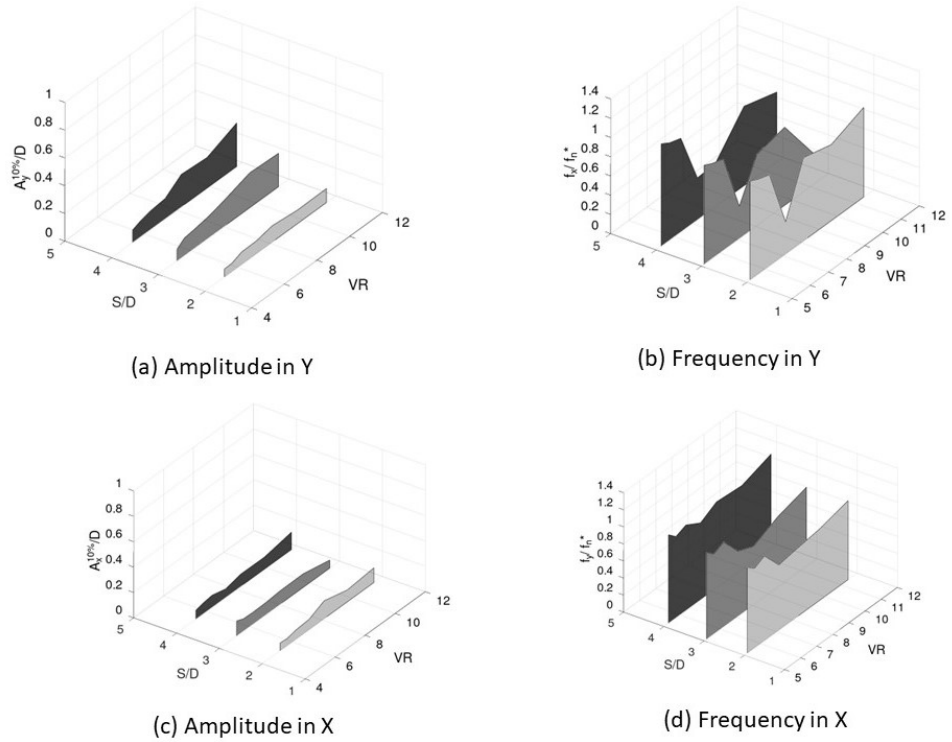

Figure 5. Results of 4-column arrays with $\theta = 0°$: (a) $A_y^{10\%}/D$, (b) $f_y^* = f_y/f_n$, (c) $A_x^{10\%}/D$ in, and (d) $f_x^* = f_x/f_n$.

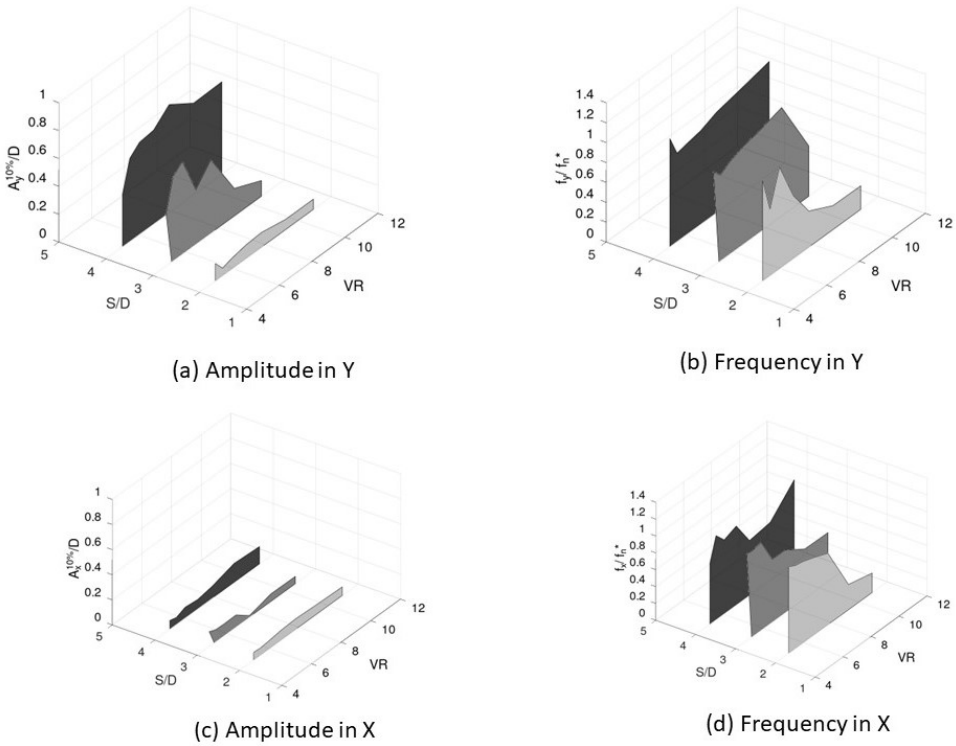

Figure 6. Results of 4-column arrays with $\theta = 45°$: (a) $A_y^{10\%}/D$, (b) $f_y^* = f_y/f_n$, (c) $A_x^{10\%}/D$ in, and (d) $f_x^* = f_x/f_n$.

Figure 6 shows the results of the amplitudes (a and c) and frequencies (b and d) for in-line and cross-flow directions with arrangements composed of four columns of square section, considering 45°of flow incidence. Considering the dimensionless amplitudes in the cross-flow direction, this is the case with the largest differences found, while for $S/D = 2$

such amplitudes do not exceed $A_y^{10\%}/D = 0.2$, for larger distances between columns this value grows considerably, characterizing itself as a worrying arrangement in terms of operation as SSP or FOWT.

Figs. 7, 8 and 9 show time histories of displacement in the X and Y directions for an arrangement with three columns of square section, respectively, for the reduced velocities 5.33, 8.35 and 11.76. As mentioned, the presence of two resonance mechanisms is observed, one at lower reduced speeds and the other at higher reduced velocities, with a loss of synchronization in the intermediate range.

When performing a temporal analysis of structures subjected to fluid flow, it is possible to observe distinct periodic oscillations, with characteristic frequencies corresponding to the FIV modes, which are in accordance with their widely documented characteristics. In this context, the flow triggers the formation of vortices, resulting in cyclic forces that affect the structure and cause its oscillatory response. The regularity and periodicity observed in the temporal record data strongly corroborate the occurrence of FIV, evidencing its significant influence on the structural dynamics.

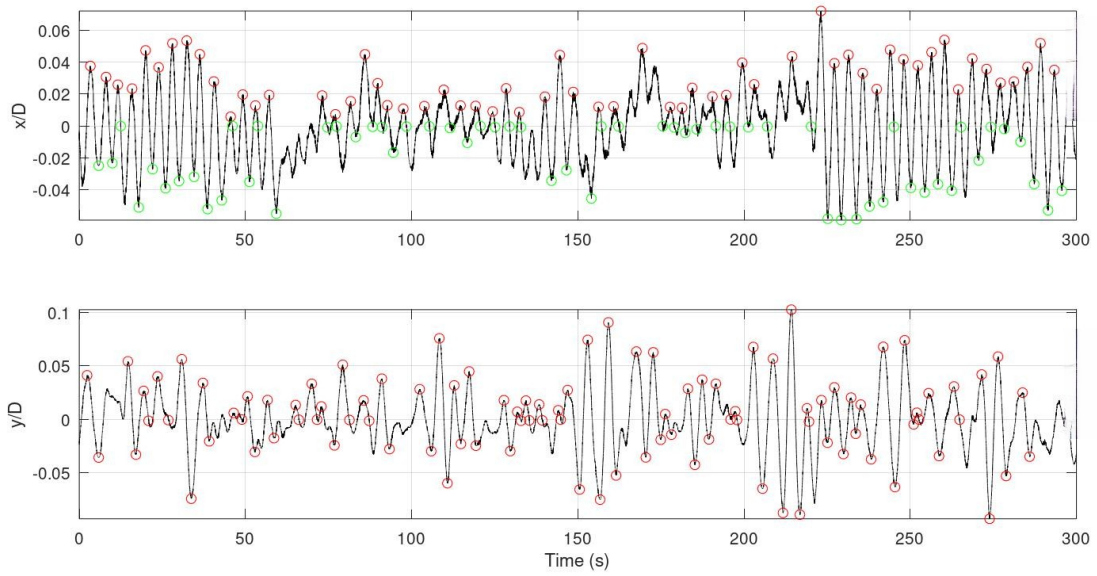

Figure 7. Time-histories of inline and cross-flow displacements, 3-column array, $\theta = 90°$, $Vr = 5.33$.

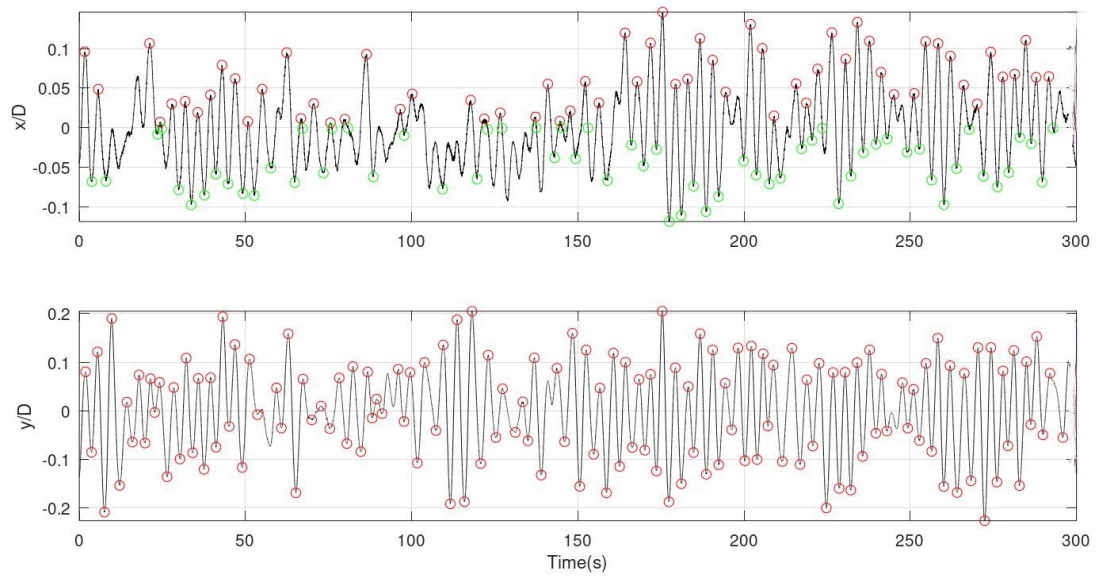

Figure 8. Time-histories of inline and cross-flow displacements, 3-column array, $\theta = 90°$, $Vr = 8.35$.

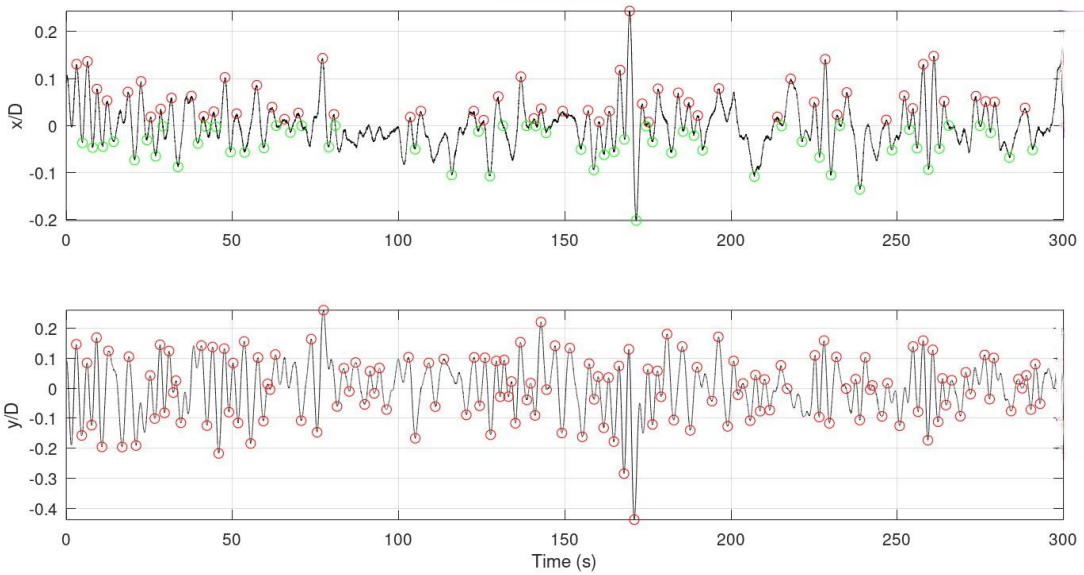

Figure 9. Time-histories of inline and cross-flow displacements, 3-column array, $\theta = 90°$, $Vr = 11.76$.

4. CONCLUSIONS

This article complements the FIV tests of ultrareduced models of floaters, for Semi-Submersible Platforms (SSP) or Floating Offshore Wind Turbines (FOWT) applications, carried out at LIFE-UFSC-Joinville using arrangements of three and four columns of square section. The tests aimed to investigate the effects of the angle of flow incidence. Three different angles of attack were tested for the three-column arrays and two different angles of attack for the four-column arrays, covering a reduced velocity range from 4.69 to 11.87, which corresponds to a Reynolds number range from 597.5 to 1317.5. The main results obtained refer to the amplitudes and frequencies in the transverse directions and along the flow.

The most significant amplitudes obtained were $A_y^{10\%}/D = 0.78$ for the four-column arrangement of relative distance $S/D = 4$ and 45°of flow incidence.

The aspects addressed in this study, such as different arrays and the effects of the angle of attack of the fluid flow, proved to be determining factors in the behavior of the FIV and should be considered during the design phase. In practice, a typical platform operation occurs in lower reduced speed ranges. In the specific context of FIV, the best solution, regardless of cross section and position, is to keep the smallest distance between the columns $S/D = 2$, as this results in the smallest range of motion.

As in Part 1, dealing with circular column arrangements, the results presented here confirm their pertinence, not only as material for a better validation of numerical simulations but also serve to show that tests in low Reynolds number regimes can be helpful in the screening large sets of options, proving to be time- and cost-effective.

5. ACKNOWLEDGEMENTS

This study was funded by the National Council for Scientific and Technological Development (CNPq), finance code 437114/2018-0. The last author also thanks CNPq for the individual research grant, code 314057/2021-8.

6. REFERENCES

Blevins, R.D., 2001. *Flow-Induced Vibration*, Krieger Publishing Company. 2nd edition. ISBN 1575241838.

Bruner, M.E., Soares, K.G., Dittrich, G.P. and Fujarra, A.L.C., 2023. "Experiments of flow-induced vibration no models in rigimes of low reynolds numbers: Part 1 – square-columns arrangements". In *Proceedings of the 27th International Congress of Mechanical Engineering - COBEM 2023*. Florianópolis, Brazil.

Fujarra, A.L.C., Rosetti, G.F., de Wilde, J. and Gonçalves, R.T., 2012. "State-of-art on vortex-induced motion: A comprehensive survey after more than one decade of experimental investigation". In *Proceedings of the 31st International Conference on Ocean, Offshore and Arctic Engineering – ISOPE2012*. American Society of Mechanical Engineers – ASME, Rio de Janeiro, Brazil.

Nemes, A., ZHAO, J., Lo JACONO, D. and SHERIDAN, J., 2012. "The interaction between flow-induced vibration mechanisms of a square cylinder with varying angles of attack". *Journal of Fluid Mechanics*, Vol. 710, p. 102–130.

doi:10.1017/jfm.2012.353.

Paidoussis, M.P., PRICE, S.J. and de LANGRE, E., 2013. *Fluid-Structure Interactions: Cross-Flow-Induced Instabilities*, Cambridge University Press, p. 414. 1st edition. ISBN 1107652952.

7. RESPONSIBILITY NOTICE

The authors are solely responsible for the printed material included in this paper.